THE ASTROPHYSICAL JOURNAL, 563:451–461, 2001 December 10

LARGE-APERTURE [O I] 6300 Å PHOTOMETRY OF COMET HALE-BOPP: IMPLICATIONS FOR THE PHOTOCHEMISTRY OF OH

JEFFREY P. MORGENTHALER,[1] WALTER M. HARRIS,[2] FRANK SCHERB,[1,3] CHRISTOPHER M. ANDERSON,[4] RONALD J. OLIVERSEN,[3,5] NATHANIEL E. DOANE,[3,6,7] MICHAEL R. COMBI,[8] MAXIMUS L. MARCONI,[9] AND WILLIAM H. SMYTH[10]

Received 2001 April 17; accepted 2001 August 10

ABSTRACT

Large-aperture photometric observations of comet Hale-Bopp (C/1995 O1) in the forbidden red line of neutral oxygen ([O I] 6300 Å) with the 150 mm dual-etalon Fabry-Pérot spectrometer that comprises the Wisconsin Hα Mapper and a 50 mm dual-etalon Fabry-Pérot spectrometer at the McMath-Pierce main telescope from 1997 late February to mid April yield a total metastable O(^1D) production rate of (2.3–5.9) × 10^{30} s^{-1}. Applying the standard H_2O and OH photodissociation branching ratios found in Huebner, Keady, & Lyon and van Dishoeck & Dalgarno, we derive a water production rate, $Q(H_2O)$, of (2.6–6.1) × 10^{31} s^{-1}, which disagrees with $Q(H_2O) \approx 1 \times 10^{31}$ s^{-1} determined by independent H_2O, OH, and H measurements. Furthermore, our own [O I] 6300 Å observations of the inner coma (<30,000 km) using the 3.5 m Wisconsin-Indiana-Yale-NOAO telescope Hydra and Densepak multi-object spectrographs yield $Q(H_2O) \approx 1 \times 10^{31}$ s^{-1}. Using our [O I] 6300 Å data, which cover spatial scales ranging from 2,000 to 1×10^6 km, and a complementary set of wide-field ground-based OH images, we can constrain the sources of the apparent excess O(^1D) emission to the outer coma, where photodissociation of OH is assumed to be the dominant O(^1D) production mechanism. From production rates of other oxygen-bearing volatiles (e.g., CO and CO_2), we can account for at most 30% of the observed excess O(^1D) emission. Since even less O(^1D) should be coming from other sources (e.g., electron excitation of neutral O and distributed nonnuclear sources of H_2O), we hypothesize that the bulk of the excess O(^1D) is likely coming from photodissociating OH. Using the experimental OH photodissociation cross section of Nee & Lee at Lyα as a guide in modifying the theoretical OH cross sections of van Dishoeck & Dalgarno, we can account for ≈60% of the observed O(^1D) excess without requiring major modifications to the other OH branching ratios or the total OH photodissociation lifetime.

Subject headings: comets: individual (Hale-Bopp 1995 O1, Hyakutake (C/1996 B2)) — instrumentation: spectrographs — molecular processes

1. INTRODUCTION

The release of water from the nucleus and its subsequent photochemical behavior drive much of the physical phenomena in cometary comae when comets approach within ~2 AU of the Sun. Thus, one of the first tasks in understanding any cometary system is to determine the water production rate, $Q(H_2O)$.

Direct infrared emission from water has been detected (e.g., Mumma et al. 1996; Dello Russo et al. 2000), but traditionally, the more easily observed emissions from its daughter products (OH, H, and O) have been the primary means for determining $Q(H_2O)$. We have observed [O I] 6300 Å emission from comets C/1973 E1 (Kohoutek; Huppler et al. 1975; Scherb 1981), 1P/1982 U1 (Halley; Magee-Sauer et al. 1988, 1990; Smyth et al. 1993), C/1989 X1 (Austin; Schultz et al. 1992, 1993), C/1996 B2 (Hyakutake; J. P. Morgenthaler et al., in preparation), and C/1995 O1 (Hale-Bopp; this work) using Fabry-Pérot interferometers with resolving powers sufficient to separate the cometary [O I] line from the Earth's [O I] airglow line and nearby cometary NH_2 lines (e.g., Fig. 1). In general, we found good agreement between our results and others. Because [O I] 6300 Å emission is the result of a forbidden transition rather than fluorescence, if all these photons come from O(^1D) created during the photodissociation of H_2O and its daughter OH, $Q(H_2O)$ can be derived from the O(^1D) production rate, $Q[O(^1D)]$, using the expression

$$Q(H_2O) = \frac{Q[O(^1D)]}{BR1 + (BR2)(BR3)}, \quad (1)$$

where the BRn are the branching ratios of the H_2O photolysis reactions (e.g., Table 1). Using the $H_2O + \nu \rightarrow H_2 + O(^1D)$ and $H_2O + \nu \rightarrow OH + H$ branching ratios (BR1 and BR2) found in Huebner, Keady, & Lyon (1992), and the $OH + \nu \rightarrow O(^1D) + H$ branching ratio (BR3) found in van Dishoeck & Dalgarno (1984), we derive $Q(H_2O)$ values for Hale-Bopp that are a factor of 3–4 higher than those determined by other methods (§ 5.1). There is a wide range of H_2O branching ratio values found in the literature (e.g., Fink & Disanti 1990, BR1 = 0.082, BR2 = 0.89), but the difference between these can account for no more than 10% of the observed excess [O I]. Limiting our analysis to the [O I] 6300 Å data taken in the inner coma (<30,000 km)

[1] Department of Physics, University of Wisconsin–Madison, Madison, WI 53706; jpmorgen@alum.mit.edu.
[2] Space Astronomy Laboratory, University of Wisconsin–Madison, Madison, WI 53706.
[3] Visiting Astronomer at the National Solar Observatory, operated by the Association of Universities for Research in Astronomy, Inc., under contract to the National Science Foundation.
[4] Department of Astronomy, University of Wisconsin–Madison, Madison, WI 53706.
[5] NASA Goddard Space Flight Center, Greenbelt, MD 20771.
[6] Raytheon ITSS, 4400 Forbes Boulevard, Lanham, MD 20706.
[7] Now at Department of Astronomy, University of Wisconsin–Madison, Madison, WI 53706.
[8] Department of Atmospheric, Oceanic, and Space Sciences, University of Michigan, Ann Arbor, MI 48109.
[9] Fresh Pond Research Institute.
[10] Atmospheric and Environmental Research, Inc.

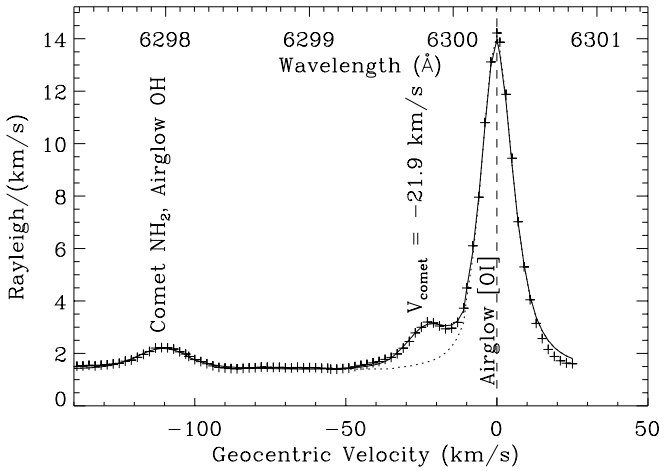

FIG. 1.—WHAM spectrum of Comet Hale-Bopp, from 1997 March 5. In this 30 s exposure, the WHAM emission-line sensitivity is less than 0.1 R. Solid line is a model with three Voigt profiles in emission plus seven Voigts in absorption representing the scattered solar spectrum. The dotted line is the same minus the cometary [O I] emission line. The wavelength of airglow [O I] line is 6300.304 Å.

where photodissociation of H_2O dominates the production of $O(^1D)$ and using the Huebner et al. (1992) H_2O branching ratios, we find $Q(H_2O)$ values consistent with others (§ 5.2). Therefore, we consider mechanisms that can produce $O(^1D)$ at large cometocentric distances, such as photodissociation of CO and CO_2. In § 6, we show that dissociation of CO and CO_2 can produce no more than $\approx$30% of the observed $O(^1D)$ and that other sources, such as electron excitation of neutral oxygen or a distributed source of H_2O in the outer coma, are unlikely to contribute significantly. Therefore, we consider the possibility that the widely accepted $OH + v \rightarrow O(^1D) + H$ branching ratio of van Dishoeck & Dalgarno (1984) may be incorrect (§ 4).

2. OBSERVATIONS

Observations of comet Hale-Bopp over a wide range of wavelengths were conducted from 1996 August 16 through 1997 April 29. Here we consider [O I] 6300 Å observations between 1997 February 22 and April 21 that were recorded by four instruments on Kitt Peak: the Wisconsin Hα Mapper (WHAM; Tufte 1997), two configurations of the 3.5 m Wisconsin-Indiana-Yale-NOAO (WIYN) telescope multiobject spectrograph (MOS), and a 50 mm dual-etalon Fabry-Pérot spectrometer coupled to the National Solar Observatory McMath-Pierce main telescope. Table 2 summarizes the capabilities of each instrument and the number of nights each observed Hale-Bopp in [O I]. The combination of MOS and Fabry-Pérot data covers spatial scales ranging from 2000 to 1×10^6 km. Table 3 gives observational details and comet ephemeris data.

The WIYN MOS absolute calibration is based on spectroscopic observations of Vega. The WHAM and 50 mm Fabry-Pérot instrument calibrations are based on the Hα surface brightness of NGC 7000 (the "North America Nebula"; coordinates $\alpha_{2000} = 20^h58^m4^s$, $\delta_{2000} = 44°35'43''$). The average surface brightness of NGC 7000 was determined by Scherb (1981) to be 850 $\pm$ 50 rayleighs (R) over the central 49′ of the nebula, where

$$1\ \mathrm{R} = \frac{10^6}{4\pi}\ \text{photons s}^{-1}\ \text{cm}^{-2}\ \text{sr}^{-1}\ . \qquad (2)$$

The Scherb (1981) NGC 7000 calibration has been verified independently by several techniques. Using a comparison blackbody source, Nossal (1994, pp. 208–212) found the Hα surface brightness of NGC 7000 to be 930 $\pm$ 80 R over a 49′ field of view (FOV), which she took to be in agreement with Scherb (1981) because of the potential for systematic error in the estimation of parasitic light contributions in Fabry-Pérot measurements of continuum sources. Furthermore, decades of work on Galactic and geocoronal Hα emissions have been based on the Scherb (1981) NGC 7000 calibration (e.g., Münch & Pitz 1989; Nossal et al. 1993; Reynolds 1997; Bishop et al. 2001).

We estimate the NGC 7000 Hα surface brightness to be $\approx$800 R over the 1° WHAM FOV, rather than 850 R, determined by Scherb (1981) for a 49′ FOV, because NGC 7000 is slightly peaked at the center of the calibration FOV (Ishida & Kawajiri 1968). By a similar argument, we estimate that the NGC 7000 surface brightness is 900 R over the 4′ FOV of the 50 mm Fabry-Pérot. The WHAM sensitivity at [O I] 6300 Å was derived from measurements of the relative transmission of the [O I] and Hα order separating filters and calculations of the transmissions of the other WHAM optical elements at [O I] and Hα. The resulting sensitivity ratio $T(6300)/T(6563)$ is 0.986 (Reynolds et al. 1998). The ratio of the transmissions of the Hα and [O I] 6300 Å order separating filters used in the 50 mm Fabry-Pérot was 1.4. We estimated the atmospheric extinction at [O I] using WHAM measurements of NGC 7000 at Hα,

TABLE 1

PHOTODISSOCIATION BRANCHING RATIOS

Reaction	BRn	Quiet Sun	Active Sun	Reference[a]
$H_2O + h\nu \rightarrow H_2 + O(^1D)$	BR1	0.050	0.067	H
$H_2O + h\nu \rightarrow H + OH$	BR2	0.855	0.801	H
$OH + h\nu \rightarrow H + O(^1D)$	BR3	0.094	...	§ 4
$OH + h\nu \rightarrow H + O(^1D)$	BR3′	0.357	...	§ 4
$OH + h\nu \rightarrow H + O(^3P)$	BR4	0.662	0.513	V
$OH + h\nu \rightarrow H + O(^3P)$	BR4′	0.472	...	§ 4
$CO(X^1\Sigma^+) + h\nu \rightarrow C(^1D) + O(^1D)$	BR5	0.046	0.042	H
$CO(X^1\Sigma^+) + h\nu \rightarrow C(^1D) + O(^1D)$	BR5′	0.123	0.123	T
$CO_2 + h\nu \rightarrow CO(X^1\Sigma^+) + O(^1D)$	BR6	0.457	0.391	H

[a] H, Huebner et al. 1992; V, van Dishoeck & Dalgarno 1984; § 4, selected values from Table 6 discussed in § 4; T, Tozzi, Feldman, & Festou 1998. The van Dishoeck & Dalgarno OH cross sections have been calculated for a heliocentric velocity of -14 km s^{-1}, appropriate for 1997 early March.

TABLE 2

INSTRUMENT CHARACTERISTICS

Name	Telescope	Bandpass (Å)	R[a]	FOV	Number of Nights
WHAM[b]	WHAM	6297–6301	30000	1°	3
Hydra MOS.....	WIYN	6100–6400	15000	45′[c]	3
Densepak MOS.....	WIYN	6100–6400	15000	28″ × 52″[d]	1
50 mm FP[b]	McMath-Pierce	6100–6400	60000	4′	9

[a] Resolving power $\lambda/\Delta\lambda$.
[b] Dual-etalon Fabry-Pérot interferometer.
[c] Ninety-six fibers, each with a 3″ FOV arrayed in six concentric rings (see Fig. 3).
[d] Hexagonal array of 91 3″ fibers on 4″ centers.

finding an extinction coefficient $K = 0.085$ mag per air mass.

3. DATA REDUCTION

3.1. *WHAM Spectra*

Our primary evidence of an unexpectedly high O(^1D) production rate in comet Hale-Bopp comes from WHAM spectroscopic observations. The spectra, one of which is shown in Figure 1, were taken with the 1° WHAM FOV centered on the head of the comet. Over such a wide FOV, the dominant feature is the airglow [O I] emission ($\sim$100 R).

The WHAM spectra (e.g., Fig. 1) were fit using a program called "Voigt-fit" developed by R. C. Woodward (University of Wisconsin). The program improves on the approximation of the Voigt profile and its derivative in Rybicki & Lightman (1979, p. 291) and Armstrong (1967). The program is capable of convolving an empirically determined instrument profile with a set of arbitrarily specified Voigt functions and up to a second-order continuum function. A nonlinear least-squares fitting algorithm finds the optimal parameters and estimates their statistical errors. We measured the instrument profile with the [O I] airglow line and used a fit to a McMath-Pierce Fourier transform spectrometer data set from 1997 February 2 to constrain the solar continuum. Using the nominal WHAM [O I] calibration appropriate for diffuse sources, we find the surface brightness in the airglow and cometary [O I] lines listed in the third and fourth columns of Table 4.

Since the comet emission did not uniformly fill the WHAM 1° FOV, it is necessary to take into consideration the variation of WHAM sensitivity with position in the aperture. Figure 2 shows the normalized sensitivity as a function of position as measured with a neon 6304 Å line projected onto a diffusing screen in the instrument calibration apparatus. The instrument is more sensitive in the center than toward the edges of the FOV; thus, for a centrally concentrated source, such as the comet, the effective instrument sensitivity was higher than if the source uniformly filled the entire aperture. We calculate the increment to the instrument sensitivity for each night by multiplying the image in Figure 2 by the normalized comet image from each night (e.g., Fig. 3) and finding the average pixel value of the resulting image. These increments to the instrument sensitivity, shown in the fifth column of Table 4, are applied to the nightly average [O I] surface brightness values given in the sixth column.

TABLE 3

OBSERVATIONS

Date (UT)	Time[a] (UT)	Air Mass[a]	Instrument[b]	R_{helio}[c]	Δ[c]	$\dot{\Delta}$[d]	P.A.[e]
1997 Feb 22	11:45/15:43	5.31/2.34	W	1.129	1.594	−30.2	326.3
1997 Feb 24	11:26/12:43	7.24/2.62	W	1.110	1.560	−29.1	327.0
1997 Mar 2	11:37/13:08	5.16/2.14	H96	1.055	1.467	−24.4	330.7
1997 Mar 5	11:55/12:58	4.16/2.35	W	1.029	1.427	−21.9	333.4
1997 Mar 9	12:15/12:25	3.49/3.33	FP	0.999	1.383	−17.6	338.2
1997 Mar 10.....	11:41/12:12	5.30/3.66	FP	0.992	1.373	−16.5	338.3
1997 Mar 16.....	12:16/12:58	4.21/2.88	H96	0.956	1.330	−8.42	349.6
1997 Mar 18.....	12:07/13:04	5.04/2.88	D	0.946	1.322	−5.66	353.6
1997 Apr 7.....	03:24/03:50	3.45/4.46	FP	0.920	1.408	19.6	37.8
1997 Apr 8.....	03:30/03:38	3.53/3.68	FP	0.923	1.420	20.5	39.7
1997 Apr 9.....	03:22/03:33	3.23/3.48	FP	0.925	1.431	21.3	42.4
1997 Apr 10	03:50/04:00	4.30/4.63	FP	0.928	1.444	21.2	44.1
1997 Apr 13	03:23/03:35	3.19/3.59	FP	0.939	1.484	24.3	49.1
1997 Apr 14	02:13/03:43	1.93/3.90	FP	0.943	1.497	25.0	51.2
1997 Apr 16	02:28/02:40	2.09/2.27	FP	0.952	1.526	26.1	44.1
1997 Apr 21	02:41/03:39	2.29/3.72	H96	0.981	1.604	27.9	61.9

[a] Begin/end.
[b] W = WHAM; H96 = Hydra, 96 fibers; FP = 50 mm Fabry-Pérot; D = Densepak.
[c] In units of AU; R_{helio} is the distance between the Sun and the comet, Δ is the distance between the Earth and the comet.
[d] In units of km s^{-1}.
[e] Position angle of the anti-Sun vector, measured counterclockwise from the north celestial pole in degrees.

TABLE 4

WISCONSIN Hα MAPPER COMET HALE-BOPP SURFACE BRIGHTNESS[a]

Date (UT)	Time (UT)	Airglow[b]	I_{6300}[b,c]	IS[d]	[O I] Average[b,e]
1997 Feb 22.....	11:45	191	16.5 ± 1.9	1.22	13.3 ± 0.6
1997 Feb 22.....	12:46	129	16.1 ± 1.0		
1997 Feb 22.....	15:43	172	16.1 ± 0.6		
1997 Feb 24.....	11:26	97	19.3 ± 1.8	1.26	15.1 ± 1.2
1997 Feb 24.....	11:56	135	18.2 ± 3.2		
1997 Feb 24.....	12:43	124	19.5 ± 2.4		
1997 Mar 5	12:00	124	28.7 ± 2.3	1.28	22.5 ± 1.8

[a] Averaged over a 60′ FOV.
[b] The $\lambda = 6300$ Å surface brightness in rayleighs.
[c] Uncorrected for nonuniform FOV sensitivity; 1 σ errors.
[d] Increment due to nonuniform FOV sensitivity.
[e] Daily average, corrected for nonuniform FOV sensitivity.

3.2. *WHAM Images*

Narrowband images of Hale-Bopp in [O I] were recorded on the same nights as the WHAM spectra (Fig. 3). For the purposes of this work, we used the March 5 WHAM image shown in Figure 3 to aid with the reduction of the WHAM and 50 mm Fabry-Pérot spectroscopic data (§§ 3.1 and 3.4) and to construct radial profiles for comparison to the WIYN MOS data (§ 3.3) and model profiles. The profile of the tailward quadrant is plotted separately in Figure 7 as a thin solid line. About 13% of the total [O I] 6300 Å emission can be attributed to the tailward asymmetry seen in the [O I] image. This asymmetry is also seen in the OH image data of Harris et al. (2001) and may be related to the red wing seen in the [O I] spectral data (§ 3.4).

3.3. *WIYN MOS*

The WIYN MOS recorded up to 96 spectra simultaneously. A detailed description of the WIYN MOS reduction process used for Hale-Bopp can be found in Anderson (1999) and Glinski & Anderson (2000). As discussed in § 2, the extinction coefficient used to reduce the WHAM data was 0.085 mag per air mass. The WIYN data were reduced using the Kitt Peak standard extinction value of 0.114 mag per air mass. Thus, at a typical comet air mass of 3.6, our WIYN surface brightnesses may be 10% higher than our WHAM values. Given a typical uncertainty of at least 20% in determining extinction corrections at high air masses, we ignore these differences.

The MOS spectra were fitted using IRAF with a flat continuum and Gaussian lines. The airglow and comet lines were resolved on all nights except March 16–18. On March 16 the comet [O I] flux in the fourth ring of Hydra fibers was only a few times the sky background. The flux values in the fifth and sixth rings on March 16 were identical to

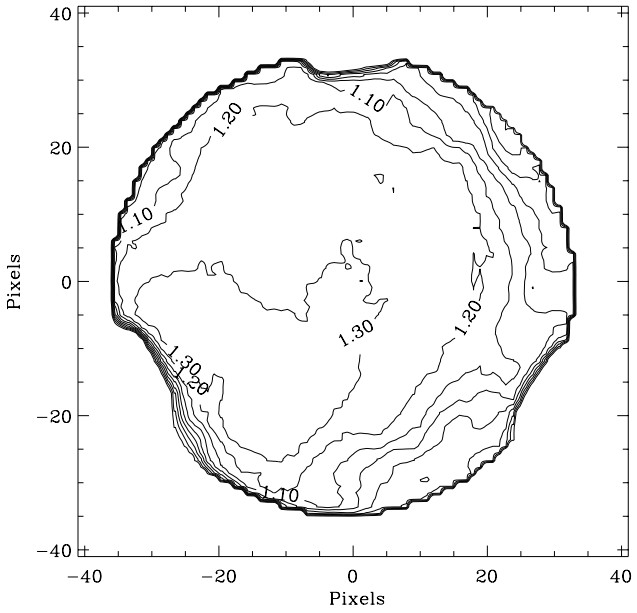

FIG. 2.—Normalized sensitivity of the 1° WHAM Fabry-Pérot FOV. Sensitivity falls off toward the edges as indicated by the contours, which are evenly spaced at intervals of 0.1. The lowest contour plotted is 0.5 and shows the outline of the spacers separating the etalons. Each pixel is 0′.8, or ≈50,000 km at $\Delta = 1.4$ AU.

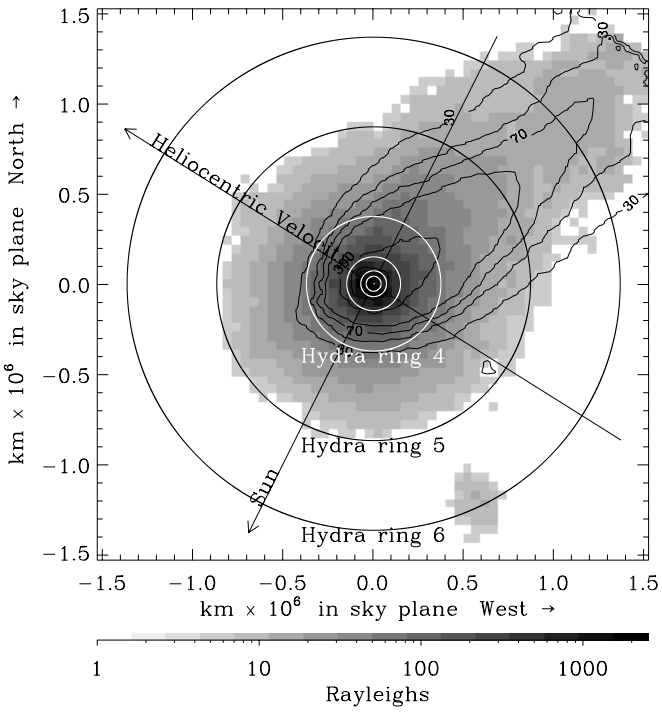

FIG. 3.—Hale-Bopp March 5 image with [O I] emission shown in gray scale, dust in contours, and circles showing positions of the Hydra annuli. The edge of the 1° WHAM FOV can be seen in the dust contours in the upper right-hand corner of the image. The angular radii of the Hydra rings are 0′.67, 1′.15, 2′.4, 6′, 14′, and 22′.

within statistical errors; thus, their average value was taken to be the sky background and subtracted from the rest of the fibers. For the Densepak observations on March 18, the fibers were arrayed within 30″ of the nucleus (30,000 km), and even a large airglow signal of several hundred rayleighs is negligible compared to the comet intensity of greater than 1×10^4 R (see Fig. 8).

3.4. *50 mm Fabry-Pérot*

This instrument was operated in a ring-sum mode, similar to that of the WHAM spectral mode, in which the Fabry-Pérot spectral fringe pattern is imaged onto a CCD. The process of extracting spectra obtained with this instrument is described in detail by Oliversen et al. (2001) and Doane (1999). The extraction process was difficult because the FOV of the McMath-Pierce main telescope was partially occulted by one of the auxiliary telescopes and the main mirror was considerably foreshortened because of Hale-Bopp's high declination. The extracted spectra were fitted with the "Voigt-fit" program described in § 3.1. A particularly good example of these spectra is shown in Figure 4. The extended red wing on the cometary [O I] line is seen in most of the 50 mm Fabry-Pérot spectra, but with a lower signal-to-noise ratio. The red wing is consistent with material flowing in the anti-Sunward direction at 5–10 km s^{-1}.

Like the WHAM, the 50 mm Fabry-Pérot did not have uniform sensitivity over its entire FOV. Instrument sensitivity variation was mapped by stepping the image of a star at regular intervals along the declination and right ascension axes. These data were interpolated using spline functions and normalized to create the image shown in Figure 5. From this we determine the effective FOV diameter to be 4′.

Since we do not have image data for all of the nights that 50 mm Fabry-Pérot data were taken, we use the March 5 WHAM data to estimate the increment to the sensitivity of the 50 mm instrument. Following the WHAM analyses, we multiply Figure 5 by the March 5 WHAM image and calculate the average pixel value of the resulting image. In this way, we find the increment to the 50 mm Fabry-Pérot sensitivity to be 1.5. The third column of Table 5 gives the sensitivity-corrected average [O I] surface brightness values, in rayleighs, over the 50 mm Fabry-Pérot FOV. The

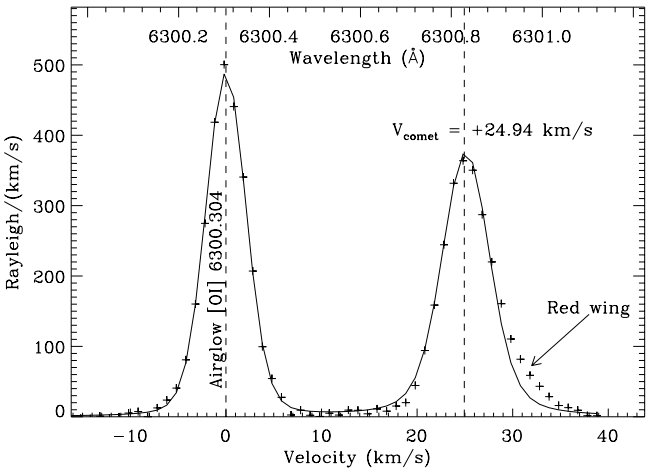

FIG. 4.—The 50 mm Fabry-Pérot spectrum of comet Hale-Bopp on 1997 April 14. The field of view is 200,000 km in radius, centered on the comet head.

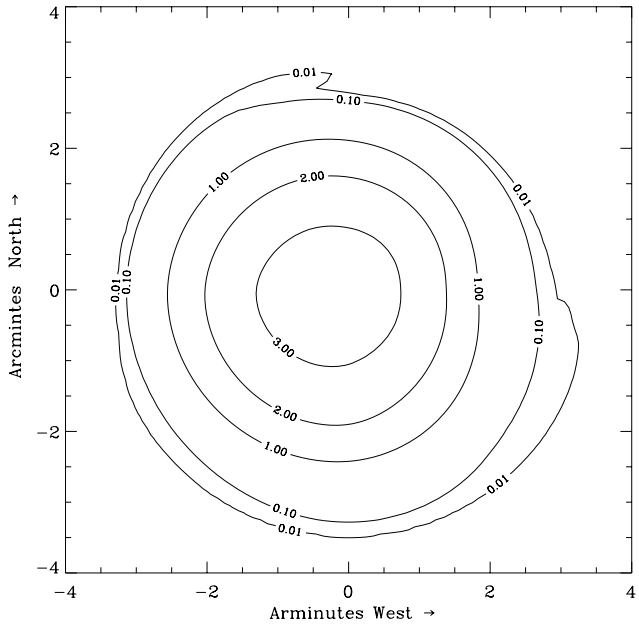

FIG. 5.—The 50 mm Fabry-Pérot field of view sensitivity map. Map is normalized so that average of the nonzero pixel values is 1.

scatter in the data, presumably due to the difficult spectral extraction process, is large (e.g., ~50% on April 7).

4. SOLAR PHOTODISSOCIATION OF H_2O AND OH

According to Keller (1976), Biermann & Trefftz (1964) were the first to discuss the importance of molecular photo-

TABLE 5

50 MILLIMETER FABRY-PÉROT SPECTROMETER HALE-BOPP SURFACE BRIGHTNESS[a]

Date (UT)	Time (UT)	I_{6300}[b,c]
1997 Mar 9	12:20	2751 ± 171
1997 Mar 10.....	12:05	2417 ± 117
1997 Mar 10.....	12:12	2514 ± 135
1997 Apr 7.....	03:35	3896 ± 154
1997 Apr 7.....	03:40	4793 ± 171
1997 Apr 7.....	03:46	3663 ± 85
1997 Apr 7.....	03:50	3094 ± 179
1997 Apr 8.....	03:30	3416 ± 82
1997 Apr 8.....	03:34	3127 ± 70
1997 Apr 9.....	03:22	2977 ± 57
1997 Apr 9.....	03:27	3273 ± 60
1997 Apr 9.....	03:30	3275 ± 101
1997 Apr 10	03:50	1624 ± 45
1997 Apr 13	03:23	1543 ± 92
1997 Apr 13	03:30	1593 ± 88
1997 Apr 13	03:35	1857 ± 103
1997 Apr 14	02:19	1935 ± 48
1997 Apr 14	02:25	2257 ± 103
1997 Apr 14	03:38	1809 ± 73
1997 Apr 14	03:43	1654 ± 79
1997 Apr 16	02:28	2870 ± 104
1997 Apr 16	02:34	2554 ± 91
1997 Apr 16	02:40	2414 ± 79

[a] Averaged over a 4′ FOV.

[b] The $\lambda = 6300$ Å surface brightness in rayleighs.

[c] Corrected for nonuniform FOV sensitivity.

dissociation as the source of the forbidden [O I] lines at 5577, 6300, and 6364 Å. Collisional excitation into the $O(^1S)$ and $O(^1D)$ states from which these emissions occur is unlikely to be the dominant source because of the low density over most of the volume of most cometary comae. Therefore, Biermann & Trefftz proposed that the excited oxygen was the result of molecular dissociations. The most likely parent molecule was H_2O, which for some time had been assumed to be the major constituent of cometary nuclei (e.g., Delsemme & Swings 1952). Owing to the molecular source of [O I], Biermann & Trefftz correctly predicted that comets would also be bright in Lyα. If H_2O was the major parent molecule, bright OH emissions were also implied. Early UV observations of comets confirmed these predictions (e.g., Code, Houck, & Lillie 1970, 1972). Water was unambiguously proven to be the major volatile component of comets by direct detection of water in comet Halley (e.g., Krankowsky et al. 1986; Mumma et al. 1986).

Using the molecular photochemistry known at the time (e.g., Potter & del Duca 1964; Jackson & Donn 1968), Bertaux, Blamont, & Festou (1973) considered several models of the observed Lyα spatial distribution in comets Bennett (C/1969 Y1) and 2P/Encke. They found that a reasonable fit to the data could be obtained using the thermal model of Mendis, Holzer, & Axford (1972) with an effective average H-atom outflow of 8 km s^{-1}. However, rather than a purely thermal distribution, Bertaux et al. preferred to construct a velocity distribution of H-atoms based on excess energies of photodissociations, which produced a similar overall result but which seemed more physically realistic. Bertaux et al. (1973) discuss in detail various excess energy states of H_2O photodissociation. Meier et al. (1976) used a similar velocity distribution to successfully fit comet C/1973 E1 Kohoutek Lyα data. High spectral resolution Hα measurements have confirmed the predominance of the 8 km s^{-1} velocity component (e.g., Huppler et al. 1975; Smyth, Marconi, & Combi 1995b). One of the implications of the H-atom velocity distributions used by Bertaux et al. and Meier et al. is that OH photodissociation, which dominates the production of H-atoms in the outer coma, must produce mostly 8 km s^{-1} H-atoms, whereas most of the OH photodissociation reactions known at the time produced H-atoms with excess velocities of greater than 20 km s^{-1}. A predissociation reaction was therefore proposed in which ground state $OH(X^2\Pi)$ is excited to the $A^2\Sigma^+(v' = 2, N' = 1)$ or higher state by a solar photon in the wavelength range 2450–2640 Å and then spontaneously enters a repulsive state such as $^2\Sigma^-$ because of a potential crossing. The predissociation reaction produces $O(^1P)$ and imparts a velocity of 8–9 km s^{-1} to the hydrogen atom (Keller 1976). Schleicher & A'hearn (1982) calculated the heliocentric velocity dependence of OH predissociation in comets, which is caused by the relative shifting of superposition of photoabsorption features with absorption features in the near-UV solar spectrum. They later updated this calculation with improved oscillator strengths and solar spectral fluxes (Schleicher & A'Hearn 1988).

Keller (1976) notes that although the predissociation reaction can account for much of the total OH cross section, it alone is not sufficient to explain the total OH solar photodissociation lifetime. Van Dishoeck, Langhoff, & Dalgarno (1983) and van Dishoeck & Dalgarno (1983, 1984) suggested that far-UV photons in the wavelength range of 1200–1800 Å could also dissociate OH by absorption into a number of other electronic states, primarily $1^2\Sigma^+$, $1^2\Delta$, $B^2\Sigma^+$, and $2^2\Pi$–$3^2\Pi$. The last three are dominated by absorption of solar Lyα photons and produce O atoms in the ^1D and ^1S states. They estimated the photoabsorption cross sections into these excited electronic states, combining them with the solar fluxes for typical solar minimum and maximum cases and the published predissociation rates of Schleicher & A'hearn (1982) to present a complete picture of dissociation of OH in comets. The total yield of $O(^1D)$ atoms is given by the combination of ^1D and ^1S branches, because O atoms produced in the ^1S state first emit the green line at 5577 Å, leaving them in the ^1D state, which then emits one of the red lines.

Laboratory measurements of the OH photoabsorption cross section by Nee & Lee (1984) were a factor of 2–3 larger than the values suggested by van Dishoeck & Dalgarno (1984) in the 1400–1800 Å region but up to 10 times larger near Lyα. However, Nee & Lee noted there was a 60% uncertainty in their absolute calibration. When combined with the 20% uncertainty in the theoretical cross sections, they concluded that the theory and experiment were actually, but only barely, in formal agreement despite the large difference in the mean absolute values and their impact on estimating dissociation rates and branching ratios for OH in comets.

Huebner et al. (1992) provided total destruction rates and the various branching ratios for OH products for solar minimum and maximum conditions using both the theoretical and experimental sets of cross sections and incorporating the effect of photoionization. Their calculations were not based on the newer version of the OH predissociation rates by Schleicher & A'Hearn (1988). Because of the large calibration uncertainty in the experimental values and the very small value implied for the total OH photodissociation lifetime, which seems contradictory to many OH observations (Budzien, Festou, & Feldman 1994), Huebner et al. assigned a poor quality factor to their experimental version of OH photodestruction but a good one to the theoretical version.

It is clear that the solar Lyα flux is important in any assessment of OH photodissociation but especially for the $O(^1D)$ yield. Daily measures of the solar Lyα flux are available from the *Upper Atmosphere Research Satellite* SOLSTICE instrument throughout the Hale-Bopp apparition (Woods et al. 1996). None of the published calculations for OH destruction and $O(^1D)$ yield include up-to-date numbers for all of the relevant processes, and the question of the absolute value of the far-UV cross section, especially at Lyα, still seems unresolved. We construct several scenarios for the modification of the OH photodissociation cross section based on the van Dishoeck & Dalgarno and Nee & Lee cross sections and updated predissociation rates and solar Lyα fluxes. The resulting $OH + \nu \rightarrow O(^1D)$ branching ratio (BR3), yield of 8 km s^{-1} H atoms (BR4), and OH lifetime (τ_{OH}) are summarized in Table 6 along with existing published values.

The first two rows of Table 6 show the BR3, BR4, and τ_{OH} values calculated by van Dishoeck & Dalgarno (1984) and by Huebner et al. (1992) using the van Dishoeck & Dalgarno (1984) cross sections but a slightly different solar spectrum. In the third row, labeled "VD + S88," we use the absolute cross sections of van Dishoeck & Dalgarno, the updated predissociation calculations of Schleicher & A'Hearn (1988), the OH photoionization rate given in

TABLE 6

QUIET-SUN OH PHOTODISSOCIATION CALCULATIONS

Reference[a]	BR3[b]	BR4[c]	τ_{OH}[d]
VD	0.048	0.718	120
H/VD	0.094	0.662	134
VD + S88 (BR3)	0.066	0.686	123
VD + S88II	0.300	0.415	123
NL + VD.....	0.183	0.600	107
NL + VDII (BR3′).....	0.357	0.472	85
H/NL	0.390	0.453	50

[a] VD, using van Dishoeck & Dalgarno 1984 theoretical OH cross sections; H/VD, treatment of VD cross sections by Huebner et al. 1992; VD + S88, VD updated for OH predissociation calculations of Schleicher & A'Hearn 1988 assuming $v_{helio} = 0$ km s^{-1} (these values are used as BR3 and BR4 in Table 1); VD + S88II, VD + S88 with BR4 at its 1σ minimum and the resulting extra photons shifted to BR3; NL + VD, Nee & Lee 1984 experimental cross sections divided by 2.5 to match VD total cross section in the 1400–1800 Å region; NL + VDII, same as NL + VD, but NL cross section at Lyα is not scaled (these values are used as BR3′ and BR4′ in Table 1); H/NL, treatment of NL cross sections in Huebner et al. 1992.

[b] OH + $h\nu \rightarrow$ H + O(^1D).

[c] OH + $h\nu \rightarrow$ H + O(^3P).

[d] OH lifetime in kiloseconds.

Huebner et al., and a solar Lyα flux of 3.0×10^{11} photons cm^{-2} s^{-1} (see Combi et al. 2000 for individual days throughout the period, corrected for the Sun's hemisphere as seen by the comet). This OH lifetime and yield of 8 km s^{-1} H atoms have been used successfully in a number of analyses of observations of the H coma that are sensitive to the H-atom velocity distribution (e.g., Combi & Smyth 1988; Combi et al. 1998, 2000).

Any calculation based on the complete set of Nee & Lee experimental cross sections produces total OH lifetimes that are too short to be compatible with cometary observations (e.g., last row in Table 6). Using the Nee & Lee cross sections, the greatest dissociation rate comes from the 1400–1800 Å region of the solar spectrum. Under the circumstances, it may be reasonable to consider that the van Dishoeck & Dalgarno (1984) cross section in this region are correct. Thus, for the case shown in row "NL + VD" of Table 6, we divide the experimental cross sections by a factor of 2.5, forcing them to agree with the 1400–1800 Å region in the van Dishoeck & Dalgarno calculation. Because the Nee & Lee cross section is much higher at Lyα, even after dividing by 2.5, the resulting cross section at Lyα is still somewhat higher than the van Dishoeck & Dalgarno value. The next case, row "NL + VDII," is the same as the previous, except we use the actual Nee & Lee cross section at Lyα. This provides an upper bound to the O(^1D) yield at the expense of making the OH lifetime and yield of 8 km s^{-1} H atoms uncomfortably low. If we use the entire experimental cross section, we would likely obtain a result similar to the experimental version of Huebner et al. (row "H/NL").

The "NL + VD" case, in which we force agreement of the Nee & Lee cross sections to the van Dishoeck & Dalgarno values in the 1400–1800 Å region, probably represents the smallest values for the OH lifetime and the yield of 8 km s^{-1} H atoms that are consistent with observations and model parameter tolerances for OH and H observations. A final consideration is to acknowledge that there is, after all, some uncertainty associated with the predissociation lifetime in the near-UV into the $A^2\Sigma^+$ state (Schleicher & A'Hearn 1988). If that rate is reduced by its 20% uncertainty below its estimated mean value but the total OH lifetime is held fixed at the level set by the second case and all the extra rate is assigned to the Lyα branches (i.e., effectively giving more weight to the large experimental cross sections), the branching ratio for O(^1D) would increase to 0.30, and the yield of 8 km s^{-1} H atoms would decrease to 0.451 (row "VD + S88II" of Table 6). This would also require shifting a third of the population of 8 km s^{-1} H atoms to 20–24 km s^{-1}. Such a shift would be less of a problem, practically, for explaining observations of comet Hale-Bopp alone, because the large collision region implies that many fast H atoms would be collisionally thermalized to lower velocities anyway (Combi et al. 2000). However, there are earlier studies of comets with much smaller collisional regions, namely, Kohoutek (Meier et al. 1976; Combi & Smyth 1988) and Halley (McCoy et al. 1992; Smyth, Combi, & Stewart 1991), which are more sensitive to the presence of lower velocity H atoms, and those are not consistent with such a large reduction in the population of 8 km s^{-1} H atoms.

5. WATER PRODUCTION RATE

5.1. *Large-Aperture Photometry*

Using the WHAM spectroscopic measurements, we determine the average surface brightness, I_{6300}, of Hale-Bopp in the [O I] 6300 Å line for the dates listed in Table 4 over the WHAM FOV, $\Omega = 2.35 \times 10^{-4}$ sr. The total production rate of O(^1D) photons, Q[O(^1D)], is then

$$Q[\mathrm{O}(^1D)] = (\tfrac{4}{3})(4\pi\,\Delta^2\Omega I_{6300})AC\ , \qquad (3)$$

where the factor of $\frac{4}{3}$ corrects for the emission in the 6364 Å decay path of O(^1D), which is outside of our bandpass, Δ is the distance between the Earth and the comet, and AC is the aperture correction.

As shown in Figure 3, the WHAM FOV was large enough so that AC is negligibly different than 1. For the 50 mm Fabry-Pérot spectrometer instrument, we calculate AC to be 2.25 by multiplying a normalized version of the March 5 WHAM [O I] image by the 50 mm instrument sensitivity map shown in Figure 5 and summing over all the nonzero pixels. In principle, the 50 mm Fabry-Pérot sensitivity and aperture corrections are functions of the water production rate and geocentric distance of Hale-Bopp. However, we ignore these effects since, as shown in Figure 6, over the time span in question, the water production rate of Hale-Bopp was relatively constant and the geocentric distance varied only $\sim$10%. The fourth column of the "W" and "FP" rows of Table 7 gives the WHAM and 50 mm Fabry-Pérot Q[O(^1D)] values derived in this way.

In previous work, we derived $Q(H_2O)$ assuming all O(^1D) was formed during the photodissociation of H_2O and its daughter OH (e.g., Magee-Sauer et al. 1990; Schultz et al. 1992; Smyth et al. 1995a). In this case, $Q(H_2O)$ is given by equation (1). The fifth and sixth columns of Table 7 give $Q(H_2O)$ derived in this way, where the fifth uses BR3 and the sixth uses BR3′. As shown by the open symbols in Figure 6, our $Q(H_2O)$ values derived with BR3 are, on average, a factor of 3–4 higher than $Q(H_2O)$ values derived by other methods (e.g., Dello Russo et al. 2000; Colom et al.

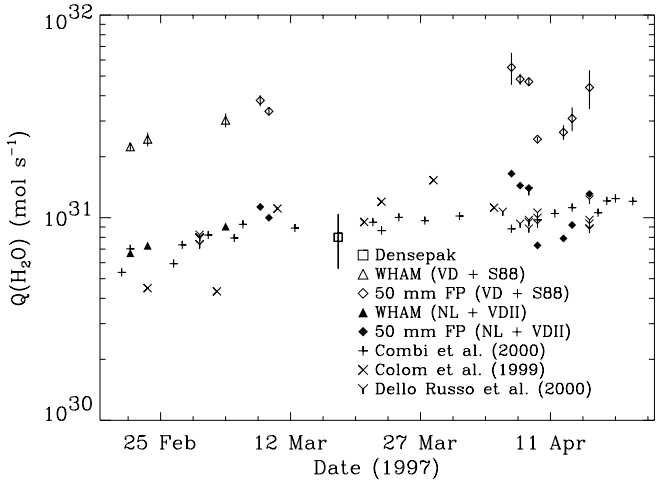

FIG. 6.—The $Q(H_2O)$ values from various works. Open symbols denote production rates derived with eq. (1), using the modified van Dishoeck & Dalgarno (1984) OH → O(^1D) branching ratio, BR3 (denoted "VD + S88" in the figure). Filled symbols are the same but with the "NL + VDII" branching ratio (BR3′) discussed in § 4.

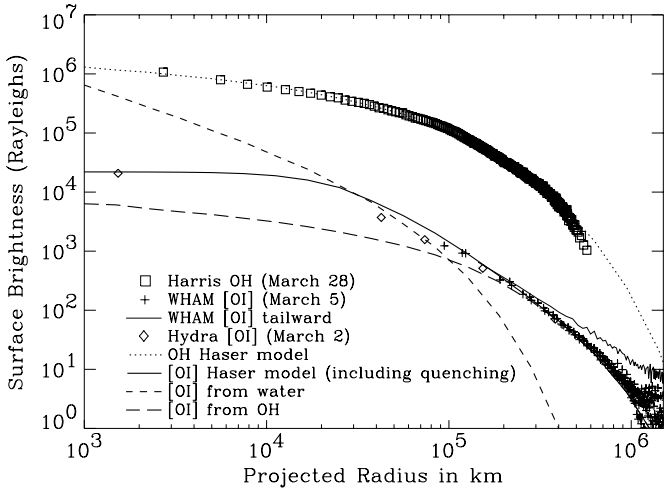

FIG. 7.—Measured and modeled radial profiles of [O I] 6300 and OH 3080 emission in comet Hale-Bopp on March 2, March 5 ([O I]), and March 28 (OH). The WHAM profile indicated with the plus symbols is created from the three quadrants of Fig. 3 away from the tailward direction; Hydra points are averaged excluding this quadrant. The good agreement between the Hydra and WHAM radial profiles at greater than 1×10^5 km is our strongest evidence of the corroboration between these data sets.

1999; Combi et al. 2000). The filled symbols in Figure 6 show that by using BR3′, we find $Q(H_2O)$ values consistent with others. As discussed in § 4, BR3′ is likely too high, suggesting that another source of [O I] 6300 Å may be present. After ruling out sources from the inner coma in § 5.2, we will consider possible contributions from the outer coma in § 6.

5.2. *Inner Coma*

We estimate $Q(H_2O)$ from the MOS data by fitting a semiempirical model to radial profiles of the data. We start with a two-component Haser (1957) model since, as shown by the upper curve in Figure 7, this model fits the OH 3080 Å data of Harris et al. (2001) over a wide range of spatial scales. Using the same H_2O and OH scale lengths (5.8×10^4 and 3.0×10^5 km, respectively), we can achieve a reasonable fit to our WHAM spatial data from March 5 and the outer two Hydra points from March 2, which cover distances greater than 1×10^5 km (Fig. 7, *plus signs and diamonds*). Not surprisingly, the production rate for this fit is very high, $Q(H_2O) = 50 \times 10^{30}$ s^{-1}.

For distances inside 1×10^5 km, where H_2O photodissociation is the dominant source of O(^1D), the Haser model fitted to the outer coma overpredicts the amount of

TABLE 7

COMET HALE-BOPP Q[O(^1D)] AND $Q(H_2O)$ VALUES[a]

Date (UT)	Instrument[b]	$R_\odot$[c]	Q[O(^1D)][d]	$Q(H_2O)$[e]	$Q'(H_2O)$[f]	Percent Error
1997 Feb 22	W	1.129	2.37	22.4	6.69	4.5[g]
1997 Feb 24	W	1.110	2.58	24.4	7.28	7.8[g]
1997 Mar 5	W	1.029	3.21	30.3	9.05	7.9[g]
1997 Mar 9	FP	0.999	4.02	37.9	11.3	6.2[g]
1997 Mar 10.....	FP	0.992	3.55	33.5	10.0	3.6[g]
1997 Mar 18.....	D	0.946	...	8	...	30
1997 Apr 7.....	FP	0.920	5.85	55.2	16.5	18[h]
1997 Apr 8.....	FP	0.923	5.12	48.3	14.4	6.2[h]
1997 Apr 9.....	FP	0.925	4.97	46.9	14.0	4.5[h]
1997 Apr 10	FP	0.928	2.59	24.4	7.3	2.7[g]
1997 Apr 13	FP	0.939	2.80	26.4	7.9	8.3[h]
1997 Apr 14	FP	0.943	3.28	30.9	9.2	13.4[h]
1997 Apr 16	FP	0.952	4.65	43.9	13.1	21.7[h]

[a] These $Q(H_2O)$ values are derived assuming that photodissociation of H_2O and its daughter OH are the only sources of O(^1D).

[b] W = WHAM; H96 = Hydra, 96 fibers; FP = 50 mm Fabry-Pérot; D = Densepak.

[c] Hale-Bopp heliocentric distance in units of AU.

[d] In units of 10^{30} s^{-1}, large-aperture case.

[e] In units of 10^{30} s^{-1}. WHAM and 50 mm Fabry-Pérot results derived with eq. (1) and OH → O(^1D) branching ratio, BR3, from the "VD + S88" row of Table 6.

[f] In units of 10^{30} s^{-1}. WHAM and 50 mm Fabry-Pérot results derived with eq. (1) and OH → O(^1D) branching ratio, BR3′, from the "NL + VDII" row of Table 6.

[g] Formal 1 σ errors from curve fit propagated through average.

[h] Standard deviation of individual values.

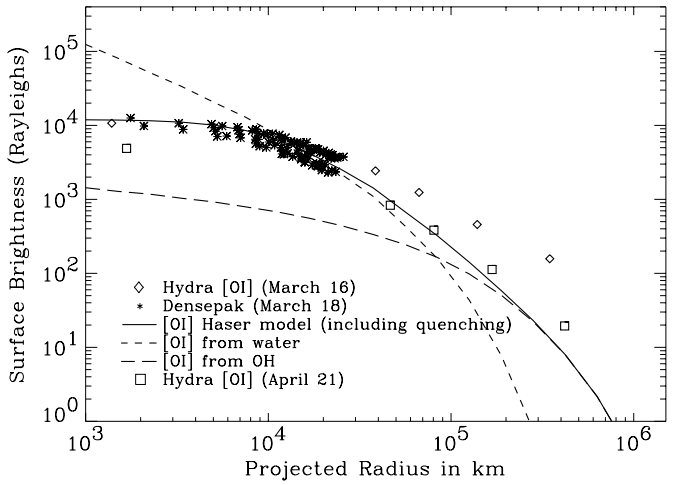

FIG. 8.—Measured and modeled radial profiles of [O I] 6300 emission in comet Hale-Bopp on March 16, March 18 (models indicated in solid and dashed lines), and April 21. Note the good agreement between the March 16 (Hydra) and March 18 (Densepak) data. We infer from this and Fig. 7 good agreement between WHAM and Densepak.

[O I]. Inside 10,000 km, the pure Haser model, shown as the short-dashed line in Figures 7 and 8, is a very poor predictor of the [O I] distribution. The fact that the OH distribution is well fitted in this area suggests that the underlying H_2O and OH populations are still reasonably well approximated by Haser distributions and that some effect is suppressing only the emission of [O I]. One likely candidate for this effect is collisional quenching of the metastable $O(^1D)$ state, thought to be dominated by collisions with H_2O. Using the standard $H_2O + O(^1D) \rightarrow O(^3P)$ quenching rate of 2.3×10^{-10} cm^3 s^{-1} found in Streit et al. (1976), we could not achieve a good fit to the data inside 10,000 km. Another possible effect leading to the underproduction of [O I] in this region is suppressed photodissociation of H_2O due to the large Lyα opacity of Hale-Bopp's inner coma. For the purposes of our empirical model, we did not compute the Lyα opacity; rather, we increased the quenching rate until a good fit was obtained. For an FOV $\gtrsim$ 50,000 km, the total number of photons lost to this exaggerated quenching rate (8×10^{-10} cm^3 s^{-1}) compared to an unquenched Haser model is negligible.

The solid-line fit to the Densepak points in Figure 8 (*asterisks*) is a two-component Haser model, including exaggerated quenching, with Haser scale lengths identical to those in Figure 7 but $Q(H_2O) = 8 \times 10^{30}$ s^{-1}, which is more consistent with $Q(H_2O)$ values determined by other methods. Also shown in Figure 8 is Hydra data from March 16 and April 21. These data are consistent with $Q(H_2O)$ values between those of Densepak and WHAM but are not well fitted by our Haser model; thus, we do not quote specific production rates for the Hydra data.

6. DISCUSSION

In § 5, we show that [O I] 6300 Å emission within $\sim$30,000 km of the nucleus of comet Hale-Bopp is consistent with independent measurements of $Q(H_2O)$. However, over the entire coma, we see 3–4 times as much [O I] 6300 Å emission as expected, given the standard model of H_2O and OH photochemistry. Although the greatest surface brightness of [O I] is found in the water-dominated nuclear region, by far the bulk of the [O I] photons come from the (presumably) OH-dominated outer coma. Assuming the other $Q(H_2O)$ measurements to be correct, we are led to one or both of the following possibilities: (1) there is a source of $O(^1D)$ in the outer coma that is unknown or has been previously ignored or (2) there is an error in the standard model of OH photochemistry previously undetected by narrower FOV measurements.

To address possibility (1), we consider the contribution of CO and CO_2 to the total amount of $O(^1D)$, since these are the most abundant oxygen-bearing volatiles after H_2O and OH. We find that it is unlikely that these species are providing more than a moderate fraction of the observed $O(^1D)$ excess. Infrared measurements of CO_2 at 2.9 AU imply $Q(CO_2)/Q(H_2O) \approx 20\%$, which is likely an upper limit for $Q(CO_2)/Q(H_2O)$ at 1 AU, because of the greater volatility of CO_2 (Crovisier et al. 1997). Weaver, Feldman, & McPhate (1994) measure a CO_2/H_2O ratio in comets P/Halley and 103P/Hartley 2 of 4%. Using the $CO_2 \rightarrow CO + O(^1D)$ branching ratio listed in Table 1, CO_2 could produce up to $\sim$25% of the observed $O(^1D)$ in comet Hale-Bopp. Radio measurements in early March imply $Q(CO)/Q(H_2O) \approx 15\%$ (Biver et al. 1999). Using the larger of the $CO \rightarrow C + O(^1D)$ branching ratios listed in Table 1, this amount of CO contributes less than 5% of the total observed $O(^1D)$ in comet Hale-Bopp. Thus, CO and CO_2 are unlikely to contribute more than 30% of the total $O(^1D)$ in comet Hale-Bopp.

We also consider the possibility that ground-state oxygen is being excited by collisions with electrons. Evidence for such collisions at distances of up to 160,000 km is found in O I] 1356 Å emission detected by McPhate et al. (1999). However, one would expect that the effect of these collisions would be greater at smaller cometocentric distances, where densities are greater, rather than greater at the large distances, as we observe. Because of the complex dependence of the [O I] 6300 Å distribution on electron density and temperature, a quantitative treatment of this subject is beyond the scope of this work. Therefore, we cannot conclusively rule out this possibility. Also complicated by temperature and density effects are the processes of dissociative recombination and collisional dissociation. However, using our Haser models, ionization cross sections from Huebner et al. (1992), and dissociative recombination rates from Le Teuff, Millar, & Markwick (2000), we estimate that these effects contribute less than 1% of the total number of [O I] 6300 Å photons in comet Hale-Bopp.

Another possible source of $O(^1D)$ in the outer coma is a distributed source of H_2O, perhaps coming from large particles ejected from the nucleus, not seen with other observing techniques. Since there is no evidence of clumps in the OH images of Harris et al. (2001) or other data reported to date, this material would have to be smoothly distributed. If this material is being continuously ejected from the nucleus, it would contribute to the flattening of the $O(^1D)$ profile that we attributed to enhanced quenching in § 5.2. However, it is difficult to explain how this material could affect the $O(^1D)$ distribution without also affecting the OH distribution. Because of the known problem with using the Haser formulation to model the inner coma, we defer to more sophisticated modeling efforts, such as those of Combi, Bos, & Smyth (1993), to conclusively determine the possible magnitude and nature of a distributed H_2O source in comet Hale-Bopp. Similarly, previously unidentified large oxygen-bearing molecules could deliver $O(^1D)$ to the outer coma. However, if this mechanism were to be the primary source

of the excess O(^1D) that we observe, the amount of oxygen delivered by these molecules would have to be on the same order with the amount of oxygen in all the H_2O released by Hale-Bopp.

The arguments above suggest that an unknown or previously ignored source of O(^1D) in the outer coma of Hale-Bopp is probably not responsible for the bulk of the excess observed [O I] 6300 Å emission and leave us with the possibility that there is an error in the standard model of OH photochemistry. This being the case, one might expect that the O(^1D) excess would have been detected in previous comets. However, the 1° FOV of WHAM is the largest used to date, able to detect all the [O I] emission from the comet. Aperture corrections for the previous, narrower FOV measurements were based on fits of models that used the standard numbers for H_2O and OH photodissociation. As seen in Figure 8, such a treatment would lead to a gross underprediction of the total amount of O(^1D) in a comet if its wide-field O(^1D) distribution were similar to that of Hale-Bopp. Preliminary analysis of data from comet Hyakutake (the only other comet observed with WHAM to date) shows excess O(^1D) emission on days when the FOV was $\sim 1 \times 10^6$ km, but not on days when the FOV was a factor of 10 smaller. However, like Hale-Bopp, Hyakutake was an active comet, and one of the other mechanisms considered above, such as an extended source of H_2O in the outer coma, may be operating. A careful review of all of our past cometary data is planned in order to more fully address this question.

7. CONCLUSION

We have collected [O I] 6300 Å data from comet Hale-Bopp with four different instruments: two Fabry-Pérot spectrometers (calibrated against NGC 7000) and two multiobject spectrographs (calibrated against Vega). Overlap in radial profiles of the MOSs and narrowband images from one of the Fabry-Pérot instruments confirms good agreement between the calibrations. Limiting our analysis to the inner 30,000 km of the coma, where H_2O photodissociation likely dominates the production of O(^1D), we find a $Q(H_2O)$ value consistent with other observational results. In the outer coma, where O(^1D) production is presumably dominated by OH photodissociation, we find a factor of 3–4 times more O(^1D) than expected from standard OH photochemistry. Using the experimental OH photodissociation cross section of Nee & Lee (1984) at Lyα, nearly all the excess O(^1D) emission can be accounted for; however, the resulting yield of 8 km s^{-1} hydrogen atoms is uncomfortably low and the OH lifetime unacceptably short (case H/NL in Table 6). Using the Nee & Lee cross section only at Lyα and the widely accepted OH cross sections of van Dishoeck & Dalgarno (1984) everywhere else, $\sim$60% of the observed O(^1D) excess can be accounted for (case NL + VDII in Table 6). The remaining 30%–40% of the [O I] photons may come from photodissociating CO and CO_2, electron collisional excitation of ground-state oxygen, a distributed source of H_2O, and/or an as yet unknown source of [O I] 6300 Å in the outer coma. The NL + VDII case results in a yield of [O I] photons and 8 km s^{-1} hydrogen atoms that is consistent with observations, but an OH lifetime of 80,000 s that is somewhat shorter than the accepted solar-quiet value of 120,000 s (e.g., van Dishoeck & Dalgarno 1984; Budzien et al. 1994). Simultaneous spectral and spatial studies of H_2O, OH, [O I], and H over a wide range of spatial scales are necessary to better constrain H_2O and OH photochemical constants using comet data. Conversely and perhaps more importantly, improved laboratory and theoretical photodissociation cross sections for H_2O and OH would lead immediately to a better understanding of the physics of cometary comae.

We would like to thank S. Tufte and L. M. Haffner for their help with data acquisition, M. Krok for conducting preliminary analysis on the Hyakutake data as part of her NASA SHARP-plus internship, J. McPhate for providing an electronic copy of Figure 1 of McPhate et al. (1999), and R. Reynolds, F. Roesler, and G. Ballester for valuable discussions. This work has been supported under NSF grant AST 96-15625, NASA grant NAG5-7952, and NASA contract NASW-97020.

REFERENCES

Anderson, C. M. 1999, Earth Moon Planets, 78, 99
Armstrong, B. H. 1967, J. Quant. Spectrosc. Radiat. Transfer, 7, 61
Bertaux, J. L., Blamont, J. E., & Festou, M. 1973, A&A, 25, 415
Biermann, L., & Trefftz, E. 1964, Z. Astrophys., 59, 1
Bishop, J., Harlander, J., Nossal, S., & Roesler, F. L. 2001, J. Atmos. Sol.-Terr. Phys., 63, 341
Biver, N., et al. 1999, Earth Moon Planets, 78, 5
Budzien, S. A., Festou, M. C., & Feldman, P. D. 1994, Icarus, 107, 164
Code, A. D., Houck, T. E., & Lillie, C. F. 1970, IAU Circ. 2201
———. 1972, in Scientific Results from the Orbiting Astronomical Observatory (OAO-2), ed. A. D. Code (NASA SP-310), 109
Colom, P., Gérard, E., Crovisier, J., & Bockelée-Morvan, D. 1999, Earth Moon Planets, 78, 37
Combi, M. R., Bos, B., & Smyth, W. 1993, ApJ, 408, 668
Combi, M. R., Brown, M. E., Feldman, P. D., Keller, H. U., Meier, R. R., & Smyth, W. H. 1998, ApJ, 494, 816
Combi, M. R., Reinard, A. A., Bertaux, J., Quemerais, E., & Mäkinen, T. 2000, Icarus, 144, 191
Combi, M. R., & Smyth, W. H. 1988, ApJ, 327, 1026
Crovisier, J., Leech, K., Bockelée-Morvan, D., Brooke, T. Y., Hanner, M. S., Altieri, B., Keller, H. U., & Lellouch, E. 1997, Science, 275, 1904
Dello Russo, N., DiSanti, M. J., Magee-Sauer, K., Novak, R., & Rettig, T. W. 2000, Icarus, 143, 324
Delsemme, A. H., & Swings, P. 1952, Ann. d'Astrophys., 15, 1
Doane, N. E. 1999, B.S. thesis, Univ. Maryland
Fink, U., & Disanti, M. A. 1990, ApJ, 364, 687
Glinski, R. J., & Anderson, C. M. 2000, in 24th IAU Meeting, Joint Discussion 1, Vol. 1, Atomic and Molecular Data for Astrophysics: New Developments, Case Studies and Future Needs (Manchester: IAU), E69
Harris, W. M., Morgenthaler, J., Mierkiewicz, E., Scherb, F., Oliversen, R., & Nordsieck, K. 2001, ApJ, submitted
Haser, L. 1957, Bull. Acad. R. Sci. Liège, 43, 740
Huebner, W. F., Keady, J. J., & Lyon, S. P. 1992, Ap&SS, 195, 1
Huppler, D., Reynolds, R. J., Roesler, F. L., Scherb, F., & Trauger, J. 1975, ApJ, 202, 276
Ishida, K., & Kawajiri, N. 1968, PASJ, 20, 95
Jackson, W. M., & Donn, B. 1968, Icarus, 8, 270
Keller, H. U. 1976, Space Sci. Rev., 18, 641
Krankowsky, D., et al. 1986, Nature, 321, 326
Le Teuff, Y. H., Millar, T. J., & Markwick, A. J. 2000, A&AS, 146, 157
Magee-Sauer, K., Roesler, F. L., Scherb, F., Harlander, J., & Oliversen, R. J. 1988, Icarus, 76, 89
Magee-Sauer, K., Scherb, F., Roesler, F. K., & Harlander, J. 1990, Icarus, 84, 154
McCoy, R. P., Meier, R. R., Keller, H. U., Opal, C. B., & Carruthers, G. R. 1992, A&A, 258, 555
McPhate, J. B., Feldman, P. D., McCandliss, S. R., & Burgh, E. B. 1999, ApJ, 521, 920
Meier, R. R., Opal, C. B., Page, T. L., Carruthers, G. R., & Keller, H. U. 1976, A&A, 52, 283
Mendis, D. A., Holzer, T. E., & Axford, W. I. 1972, Ap&SS, 15, 313
Mumma, M. J., Di Santi, M. A., Dello Russo, N., Fomenkova, M., Magee-Sauer, K., Kaminski, C. D., & Xie, D. X. 1996, Science, 272, 1310
Mumma, M. J., Weaver, H. A., Larson, H. P., Williams, M., & Davis, D. S. 1986, Science, 232, 1523
Münch, G., & Pitz, E. 1989, in IAU Symp. 139, The Galactic and Extragalactic Background Radiation, ed. S. Bowyer & C. Leinert (Dordrecht: Kluwer), 193

Nee, J. B., & Lee, L. C. 1984, J. Chem. Phys., 81, 31
Nossal, S. 1994, Ph.D. thesis, Univ. Wisconsin–Madison
Nossal, S., Reynolds, R. J., Roesler, F. L., Scherb, F., & Harlander, J. 1993, J. Geophys. Res., 98, 3669
Oliversen, R. J., Doane, N. E., Scherb, F., Harris, W. M., & Morgenthaler, J. P. 2001, ApJ, submitted
Potter, A. E., & del Duca, B. 1964, Icarus, 3, 103
Reynolds, R. J. 1997, Science, 277, 1446
Reynolds, R. J., Hausen, N. R., Tufte, S. L., & Haffner, L. M. 1998, ApJ, 494, L99
Rybicki, G. B., & Lightman, A. P. 1979, Radiative Processes in Astrophysics (New York: Wiley)
Scherb, F. 1981, ApJ, 243, 644
Schleicher, D. G., & A'hearn, M. F. 1982, ApJ, 258, 864
———. 1988, ApJ, 331, 1058
Schultz, D., Li, G. S. H., Scherb, F., & Roesler, F. L. 1992, Icarus, 96, 190
———. 1993, Icarus, 101, 95
Smyth, W. H., Combi, M. R., Roesler, F. L., & Scherb, F. 1995a, ApJ, 440, 349
Smyth, W. H., Combi, M. R., & Stewart, A. I. F. 1991, Science, 253, 1008
Smyth, W. H., Marconi, M. L., & Combi, M. R. 1995b, Icarus, 113, 119
Smyth, W. H., Marconi, M. L., Scherb, F., & Roesler, F. 1993, ApJ, 413, 756
Streit, G. E., Howard, C. J., Schmeltekopf, A. L., Davidson, J. A., & Schiff, H. I. 1976, J. Chem. Phys., 65, 4761
Tozzi, G. P., Feldman, P. D., & Festou, M. C. 1998, A&A, 330, 753
Tufte, S. L. 1997, Ph.D. thesis, Univ. Wisconsin–Madison
van Dishoeck, E. F., & Dalgarno, A. 1983, J. Chem. Phys., 79, 873
———. 1984, Icarus, 59, 305
van Dishoeck, E. F., Langhoff, S. R., & Dalgarno, A. 1983, J. Chem. Phys., 78, 4552
Weaver, H. A., Feldman, P. D., & McPhate, J. B. 1994, ApJ, 422, 374
Woods, T. N., et al. 1996, J. Geophys. Res., 101, 9541